Crosstalk Reduction between Closely Spaced Optical Waveguides by Using Higher-Order Modes

Somendu Maurya,* Radoslaw Kolkowski,† Matti Kaivola, and Andriy Shevchenko
Department of Applied Physics, Aalto University, P.O.Box 13500, Aalto FI-00076, Finland

(Received 2 May 2022; revised 19 August 2022; accepted 26 September 2022; published 31 October 2022)

Optical waveguide structures can make the state-of-the-art micro- and nanofabricated devices faster and less energy consuming. However, on-chip optical components must be placed at relatively large distances from each other, on the order of the wavelength λ, to eliminate the crosstalk between them. This makes on-chip optical structures too large to compete with their electronic counterparts. In this work, we explore the possibility of suppressing the crosstalk between closely spaced dielectric waveguides by making use of higher-order modes. We show that the crosstalk between two waveguides can be essentially eliminated, even if the waveguides are separated by a distance of $\lambda/10$ only. We also study arrays of more than two waveguides and find the conditions for the efficient crosstalk reduction in them. Our results can lead to further miniaturization of photonic integrated circuits.

DOI: 10.1103/PhysRevApplied.18.044077

I. INTRODUCTION

Silicon micro- and nanostructures are the most promising candidates for future photonic integrated circuits [1–3]. They offer the advantage of fabrication with already existing CMOS technologies along with negligible losses at telecom wavelengths [4–6]. The high refractive index of silicon enables miniaturization of on-chip optical components due to strong light confinement. However, even with silicon, the miniaturization of photonic circuits is limited by the crosstalk between neighboring optical components on photonic chips.

Plasmonic structures offer light confinement at scales much smaller than their dielectric counterparts. However, due to inherent losses associated with absorption in the metals, plasmonic waveguides have been considered less practical [7]. Hybrid plasmonic-photonic platforms propose a compromise between strong confinement of light by plasmonic structures and long propagation distances in dielectric waveguides. However, they often require complicated geometries to obtain competitive results [8–10]. Another approach to reduce the coupling between optical waveguides is based on the supercell design [11,12], in which several waveguides of slightly different geometrical parameters form a supercell that is repeated periodically. The crosstalk reduction allows the waveguide separation to be reduced down to $\lambda/2$ while retaining reasonably long crosstalk-free propagation distances. Structuring the cladding to obtain nanophotonic cloaking [13] or the use of extremely anisotropic claddings [14–17] are other strategies, setting the current state of the art in crosstalk reduction. However, these approaches rely on high-aspect-ratio structures and require complicated fabrication methods.

In this work, we show that, by using higher-order modes of standard silicon waveguides with rectangular cross sections, the crosstalk between two waveguides, separated by less than $\lambda/10$, can be fully suppressed, rendering the coupling length infinite. This results from an effective mode index degeneracy of the symmetric and antisymmetric eigenmodes of the two-waveguide system. Under this condition, the optical signal in one waveguide never couples to the other waveguide. The degeneracy is not achievable with the fundamental (zeroth-order) TE and TM modes. Using higher-order modes, the crosstalk can be suppressed for two or more waveguides in the system. We show that an array of waveguides separated by a distance on the order of $\lambda/10$ can be constructed to exhibit essentially eliminated crosstalk between the waveguides for propagation distances exceeding 100 μm.

II. CROSSTALK REDUCTION

We start by considering a silicon waveguide of a rectangular cross-section embedded in glass [see Fig. 1(a)]. The refractive index of glass is taken to be 1.5 and that of silicon (Si) is assumed to be $3.572 + 0.00051i$ at a wavelength of 1000 nm [18]. Our choice of wavelength

*somendu.maurya@aalto.fi
†radoslaw.kolkowski@aalto.fi

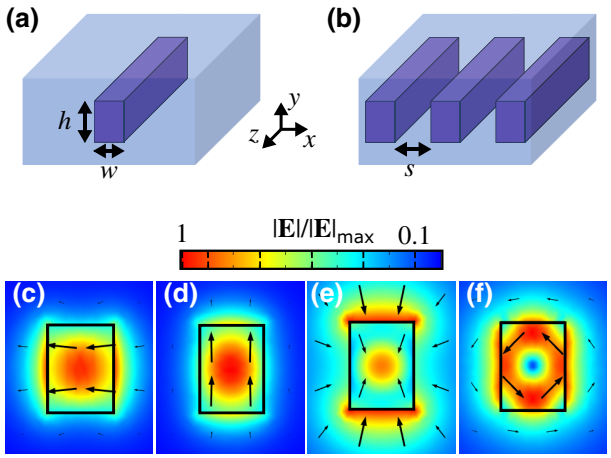

FIG. 1. Schematic illustration of an isolated waveguide (a) and a waveguide array (b). The width w, height h, and separation distance s are the parameters to be optimized. (c)–(f) Normalized transverse distribution of the electric field amplitude for the TE (c), TM (d), RA (e), and AZ (f) modes. The arrows show the orientation of the electric field vector in the transverse plane. In the presented example, the width (w) of the waveguide is 220 nm and the height (h) is 300 nm.

is arbitrary, since the approach demonstrated in our calculations is very general and could be implemented using different waveguide materials and different wavelengths. The fundamental TE and TM modes are always present in such a waveguide, but for higher-order modes to appear, the waveguide's cross section must be large enough [19]. We use COMSOL Multiphysics (mode-analysis eigenvalue solver of the wave-optics module) to find the eigenmodes of the considered waveguides and their effective mode indices. Figures 1(c)–1(f) show the electric field profiles of the fundamental (TE, TM) and the two higher-order modes. These higher-order modes are found to be radially (RA) and azimuthally (AZ) polarized [see Figs. 1(e) and 1(f), respectively]. In the provided example, the cross-section dimensions of the waveguide are $w = 220$ nm and $h = 300$ nm. From the point of view of practical realizations, such a higher-order mode could be obtained by converting a fundamental mode (either TE or TM) using a phase-shifting element, such as a gap that partially cuts the waveguide (see Ref. [20]). Other solutions are also possible [19–21].

In general, when two waveguides are positioned close to each other, light can couple from one waveguide to the other and back [22,23]. In terms of the coupled mode theory (CMT), any propagating field in the waveguides can be expanded into the eigenmodes of the system [22,24]. Mathematically, any electric field $\mathbf{E}(x,y,z)$ propagating in an assembly of N waveguides can be written as

$$\mathbf{E}(x,y,z) = \Sigma_{i=1}^{N} A_i \mathbf{E}_i(x,y) \exp(-i\beta_i z), \qquad (1)$$

where $\mathbf{E}_i(x,y)$ is the normalized electric field distribution at $z = 0$ for the ith eigenmode, and A_i and β_i are the eigenmode expansion coefficient and propagation constant of the mode, respectively. In terms of the effective mode index n_{eff}, the propagation constant is given by $\beta_i = 2\pi n_{\text{eff},i}/\lambda$, where λ is the free-space wavelength.

We refer to the eigenmodes of a system of waveguides as supermodes. Two single-mode waveguides support two supermodes. For one supermode (symmetric), the electromagnetic fields are in phase in the waveguides and for the other mode (antisymmetric), the fields oscillate out of phase (see Fig. 2). The mode excitation in a single waveguide can then be considered as a sum of the symmetric and antisymmetric supermodes with equal coefficients A_i. The beating period of the two supermodes is the coupling length (L_c), which is the propagation distance needed for the power to be entirely transferred to the other waveguide. It depends on the effective refractive indices of the symmetric and antisymmetric supermodes, n_s and n_a in accordance with

$$L_c = \frac{\lambda}{2|n_s - n_a|}. \qquad (2)$$

It can be seen that the coupling length increases to infinity, when the indices n_s and n_a approach each other.

Figure 2 shows the electric field amplitude distribution of the symmetric and antisymmetric supermodes composed of the RA and AZ modes of the individual waveguides. The effective mode indices n_s and n_a are calculated for both fundamental and higher-order modes as functions of the surface-to-surface separation s. For the TE and TM modes, these indices are seen to approach each other when the waveguide separation increases, but they never intersect [see Figs. 3(a) and 3(b)]. For the RA and AZ modes, however, we obtain an intersection point at $s = 160$ nm

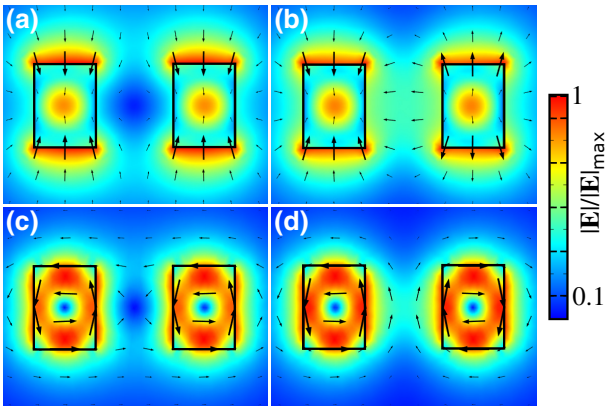

FIG. 2. Symmetric (a),(c) and antisymmetric (b),(d) supermodes of two waveguides. The RA and AZ modes are shown in the top and bottom plots. The width of each waveguide is 220 nm, the height is 300 nm, and the surface-to-surface separation of the waveguides is 280 nm.

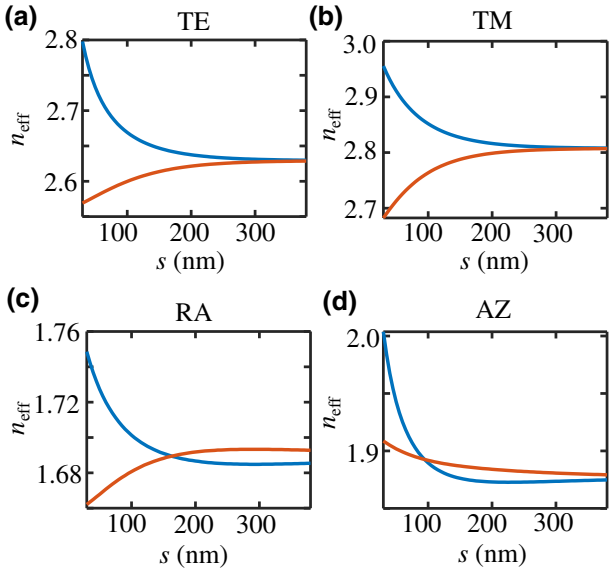

FIG. 3. Effective mode indices (n_{eff}) as functions of the separations between the two waveguides with $w = 220$ nm and $h = 300$ nm. The blue and red curves correspond to the symmetric and antisymmetric modes.

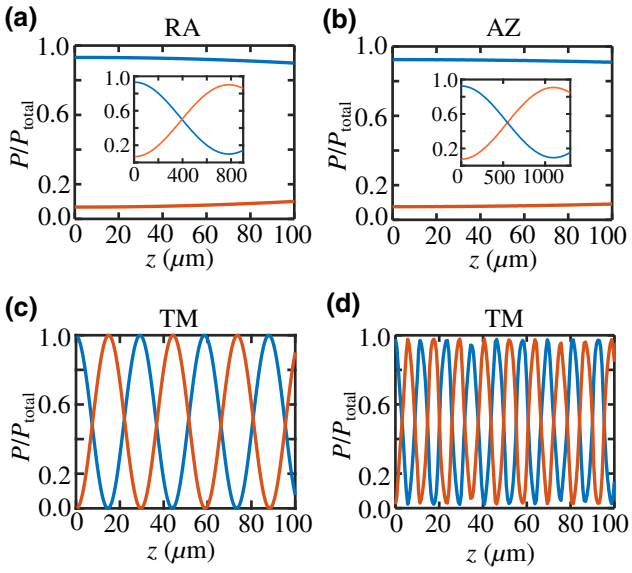

FIG. 4. Normalized optical power propagating along z in the core of the originally excited (blue) and originally dark (red) waveguide. The waveguide surface-to-surface separation is 160 nm in (a),(c) and 95 nm in (b),(d). The insets show the results of propagation over a long distance, neglecting the absorption losses in silicon.

and $s = 95$ nm, respectively [see Figs. 3(c) and 3(d)]. At these separations, the coupling length L_c is infinite and light cannot pass from one waveguide to the other.

The reason for the degeneracy of the RA and AZ supermode indices can be revealed from the field distributions of the modes. The symmetric supermodes are seen to produce a clearly visible intensity minimum in the gap between the waveguides. In the case of both RA and AZ supermodes, the fields of the symmetric supermode interfere destructively at the center of the structure and constructively at the periphery of it, while for the antisymmetric supermode, the situation is the opposite. Therefore, the symmetric supermode has more power propagating in the cladding and exhibits a lower mode index than the antisymmetric supermode does. At small separations, the gap between the waveguides becomes insignificant (not shown), and the symmetric supermode exhibits a constructive interference in the core material and a resulting higher-mode index, while the antisymmetric supermode shows the opposite.

In order to verify if the coupling length obtained from Eq. (2) is correct, we study the coupling between the waveguides numerically using COMSOL Multiphysics. For $s = 160$ nm, the supermode index difference for the RA modes is found to be 6×10^{-4}, corresponding to $L_c = 0.8$ mm. For the AZ modes, the index difference of 4×10^{-4} is obtained at $s = 95$ nm. The coupling length in this case exceeds 1 mm (5000 times the width of the waveguide). The normalized optical power in each waveguide (P/P_{total}) as a function of the propagation distance is presented in Fig. 4. At $z = 0$, essentially all the power is concentrated in the core of one of the waveguides. Upon propagation over 0.83 mm for RA modes and 1.25 mm for AZ modes, the light is fully transferred to the other waveguide, in agreement with Eq. (2). Clearly, by fine tuning the waveguide

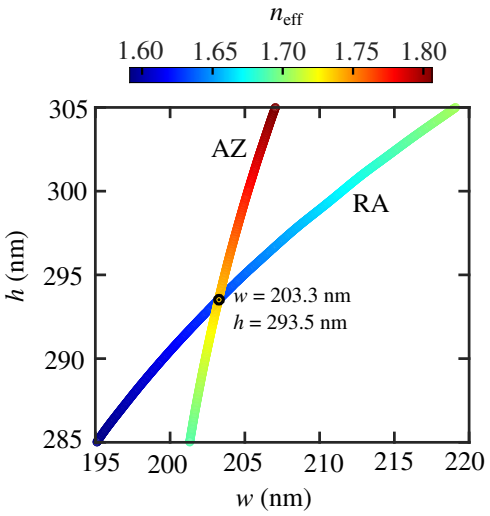

FIG. 5. The parameters w and h providing the index degeneracy condition for the RA and AZ modes at a fixed surface-to-surface separation $s = 200$ nm. The intersection point (marked by the black dot) corresponds to a single geometry of two waveguides supporting four independent channels for optical information transmission: two enabled by RA modes, and two by AZ modes.

parameters, we can increase the coupling length arbitrarily close to infinity. For comparison, Figs. 4(c) and 4(d) show the light energy transfer for $s = 160$ nm and $s = 95$ nm, respectively, for the case of TM modes (which show longer L_c than the TE modes). The calculated mode index differences are 0.03 and 0.053, respectively, and the coupling lengths are 17 and 9 μm, which are shorter by 2 orders of magnitude than L_c of the AZ and RA modes. This highlights the huge advantage offered by the higher-order modes for crosstalk-free propagation of optical signals. If in a fabricated sample, the value of s is allowed to deviate by ± 10 nm from the optimum value, the coupling length can decrease down to 250 μm for RA modes and 110 μm for AZ modes. These distances, however, are still more than 1000 times longer than s. Absorption in silicon at the considered wavelength is small and does not influence the crosstalk much. In the insets of Figs. 4(a) and 4(b), the curves are obtained by neglecting the absorption.

In Fig. 3, the eigenmode index degeneracy takes place at different separation values s for the RA and the AZ modes. However, by tuning the dimensions of the waveguides we can make the RA and AZ modes to reach the index degeneracy at the same value of s in order to double the number of independent channels for transmitting optical information. Figure 5 shows such a parametric dependence of the index degeneracy condition for the RA and AZ modes when the waveguides have a fixed separation of 200 nm. It can be seen that, for $w = 203$ nm and $h = 293$ nm, the crosstalk-free propagation distance is infinite for both RA and AZ modes. The waveguide geometries could also be optimized, e.g., to further decrease the surface-to-surface separation, or to minimize the overall footprint (including both w and h) of the waveguide system.

In a large array of waveguides, the number of independent supermodes is large as well. To achieve ideal crosstalk suppression in this case, all the supermodes should have equal effective mode indices. We did not find such index degeneracy in any system containing more than two waveguides, which makes us suppose that achieving such a condition would likely require waveguides of more complex cross-section geometries. However, for the simple rectangular geometries considered in this work, we find that, in certain ranges of geometrical parameters, the effective mode indices of the RA and AZ supermodes differ

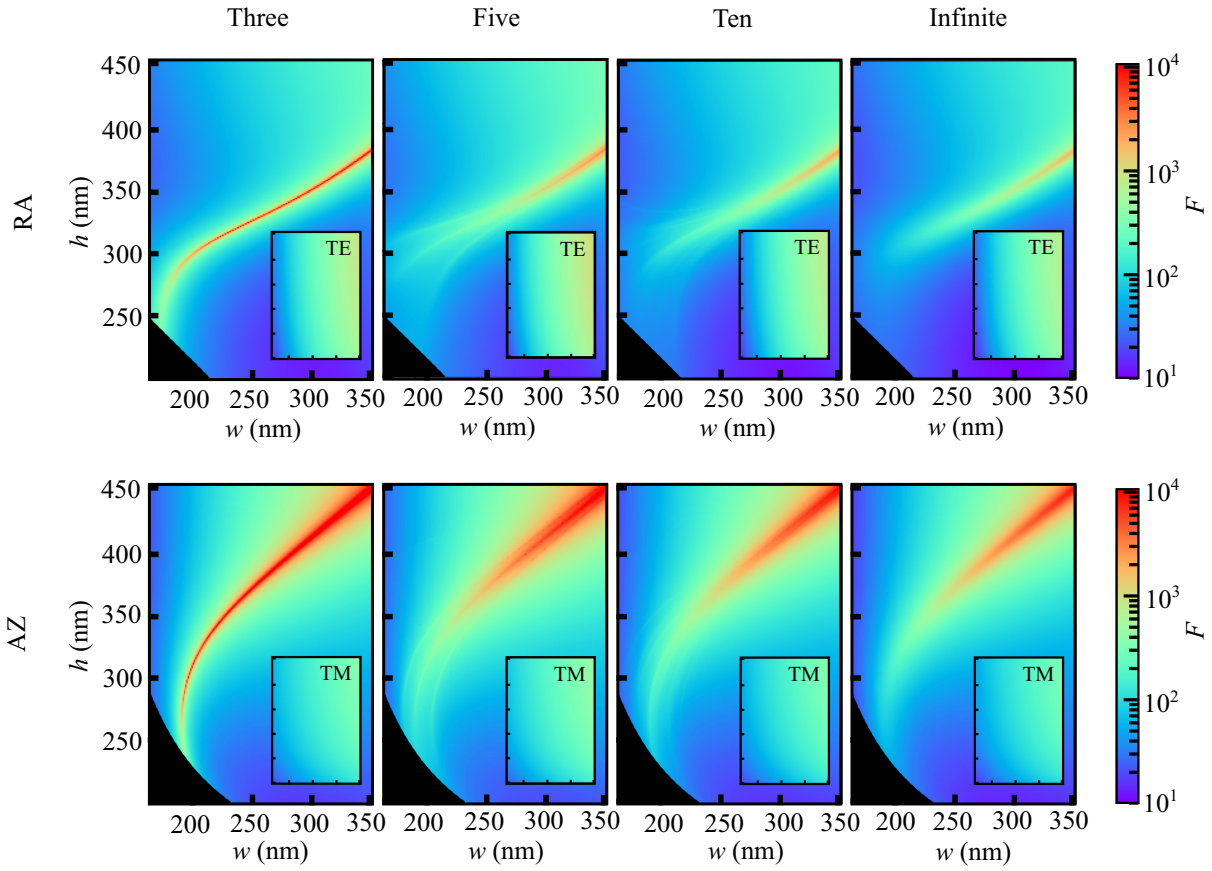

FIG. 6. Figure of merit (F) calculated for an array of three, five, ten, and an infinite number of waveguides. The top and bottom row shows the F for the RA and AZ mode excited in the central waveguide. The insets show the corresponding F for the TE and TM modes in the central waveguide.

from each other much less than the effective mode indices of the TE and TM supermodes, which can still be used for significant crosstalk reduction. The crosstalk reduction in such cases can be characterized by the following figure of merit:

$$F = \frac{\Sigma_{i=1}^{N} |A_i|^2}{\Sigma_{i>j} |n_i - n_j||A_i A_j|}. \tag{3}$$

Here, n_i is the mode index of the ith supermode and A_i is its complex expansion coefficient [see Eq. (1)] for a field localized in a single waveguide. The above expression is obtained as follows. We calculate the modulation depth ($D \propto |A_i A_j|$) and period ($L \propto \lambda/|n_i - n_j|$) for two beating supermodes i and j. In order to minimize the crosstalk, the modulation depth (D) should be minimized and modulation period (L) should be maximized. Hence, we define $G = \langle D/L \rangle / C$, where the brackets stand for averaging over all pairs of supermodes in the system and C is a normalization coefficient. To minimize the crosstalk, the function $G = \Sigma_{i>j} |A_i A_j||n_i - n_j| / \Sigma_{i=1}^{N} |A_i|^2$ should be minimized; the denominator normalizes the expression. The function to be maximized is $F = 1/G$. The larger the F, the less efficient the coupling of light to the other waveguides and the longer the coupling length.

In Fig. 6, we show the distribution of F in the w-h parameter space under fixed $s = 200$ nm for an array of three, five, ten and an infinite number of waveguides for the RA and AZ modes as well as for the TE and TM modes (see the insets). The case of infinite array is modeled using periodic boundary conditions, with different supermodes corresponding to the different in-plane Floquet momenta. Note the logarithmic color scale of the plots. In all these examples, the field is considered to be initially localized in the central waveguide (or one of the two central waveguides), and the expansion is done for this initial field profile. The plots show that, at certain values of parameters w and h, the F becomes exceptionally high, above 10^4 for the case of three waveguides and 10^3 for an infinite number of waveguides in the system. In contrast, the insets in Fig. 6 show considerably lower values of F for the TE and TM modes. Moreover, the distribution of F for the subsequent types of modes across the considered parameter space remains approximately the same for the arrays with more than five waveguides. This means that the crosstalk reduction enabled by RA and AZ modes would be equally effective in all waveguides in the bulk of the array, and only two edge waveguides can be excluded from the predicted low-crosstalk operation of the system, offering a large number of independent channels for optical information transmission.

It is useful to estimate the tolerance of the design to possible fabrication errors in the values of w and h. In Fig. 6, the region in which the figure of merit for the RA modes exceeds that of the TE modes is narrowest for the three-waveguide system, with the widths $\Delta h \approx 8$ nm and $\Delta w \approx 14$ nm in the h and w directions, respectively. This introduces a challenge for the fabrication precision. However, for more waveguides in the system, this width is larger. The AZ modes, on the other hand, show much larger tolerances, with both Δh and Δw exceeding 80 nm independently of the number of waveguides. This makes it easier to demonstrate the crosstalk reduction in practice with the AZ modes.

We analyze some examples of the considered waveguide systems in more detail. One such example is presented in Fig. 7, which shows the effective mode indices and the expansion coefficients for the three-waveguide assembly. The waveguide parameters are $w = 250$ nm and $h = 315$ nm for the RA modes, and $w = 200$ nm and $h = 320$ nm for the AZ modes. The mode indices are plotted as functions of the waveguide surface-to-surface separation s. The curves corresponding to the RA and AZ modes are seen to intersect at two different points, while the TE- and TM-mode curves, as before, do not intersect at all. Figures 7(c) and 7(f) show the supermode expansion coefficients A_i for the RA and AZ modes, respectively. At one of the crossing points in the plots (a) and (b), one of the coefficients

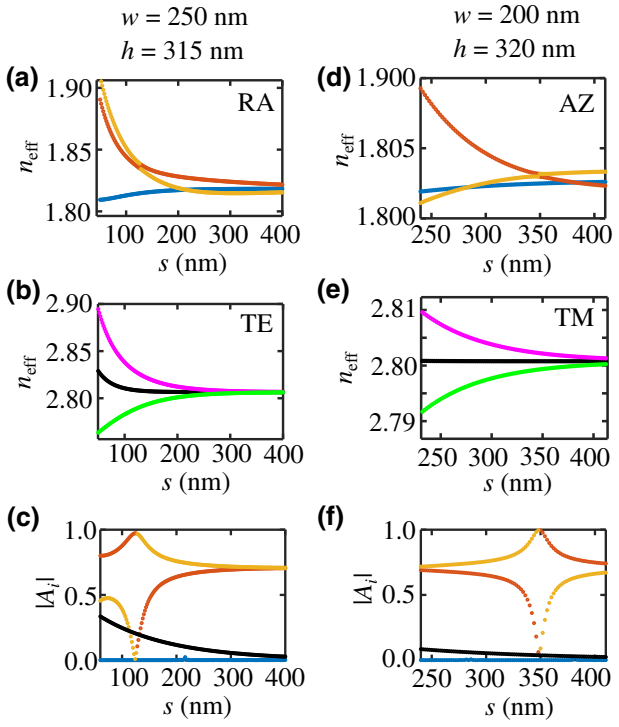

FIG. 7. Supermode indices n_i and the absolute values of the expansion coefficients A_i as a function of the surface-to-surface separation distance s between the waveguides for three-waveguide system. Plots in (a),(b) show the mode indices for the RA and TE modes, respectively, and the expansion coefficients $|A_i|$ for the RA modes are shown in (c). Plots in (d),(e),(f) show the corresponding parameters for the AZ and TM modes.

A_i becomes equal to 1. This means that one of the eigenmodes of the system coincides with the localized mode of the central waveguide. For the RA mode, this happens at $s = 120$ nm, and for the AZ mode at $s = 350$ nm.

Being the eigenmode of the system, the excitation in the central waveguide will propagate unchanged, hence offering an isolated channel for crosstalk-free optical information transmission. We also notice that the TE and TM modes may have non-negligible amplitudes (black curves in Fig. 7) once they are included in the eigenmode expansion of the RA- or AZ-mode excitation of a single waveguide. The field profiles of the supermodes contributing to the RA and AZ excitations in the central waveguide are shown in Figs. 8(a)–8(d) and 8(e)–8(h), respectively. The modes in Figs. 8(b) and 8(f) are those with A_i close to 1. The modes in Figs. 8(c) and 8(g) have only a negligible contribution to the excitation in the central waveguide (see the blue curves in Fig. 7). The modes in Figs. 8(d) and 8(h) are the TE- and TM-mode contributions that are responsible mostly for the expanded field outside the central waveguide. Hence, their influence on the power flow in the central waveguide is not significant.

We also study the propagation of different types of central-waveguide excitations (corresponding to subsequent types of modes) and the leakage of optical power from the central to the peripheral waveguides. Figure 9 shows the power flow in the central waveguide (blue curve) and in one of the side waveguides (red curve). There is a small modulation of the power in the central waveguide (less than 5%) due to coupling to the TE- and TM-like supermode. The modulation period agrees with the index difference between the supermodes. The propagation is essentially crosstalk-free for the RA and AZ modes. In contrast, the analogous analysis for the central-waveguide excitations of the TE and TM modes shows that such modes exhibit a coupling length of about 12 and 180 μm, respectively, as shown in Figs. 9(b) and 9(d).

At the end, we also investigate the propagation of single-waveguide excitations accompanied by spreading of optical power to the neighboring waveguides (discrete diffraction) inside an array of 10 waveguides, which is presented in Fig. 10. The width of each waveguide is 350 nm and the height is 450 nm. The waveguides are separated by 200-nm gaps. In Fig. 10, the light is initially coupled to the fifth waveguide from the bottom. Here, in contrast to the previous study on three waveguides, we assume pure excitations of a given mode type [pure TE modes in (a) and pure AZ modes in (b)], excluding all other types of modes from the eigenmode expansion. As can be

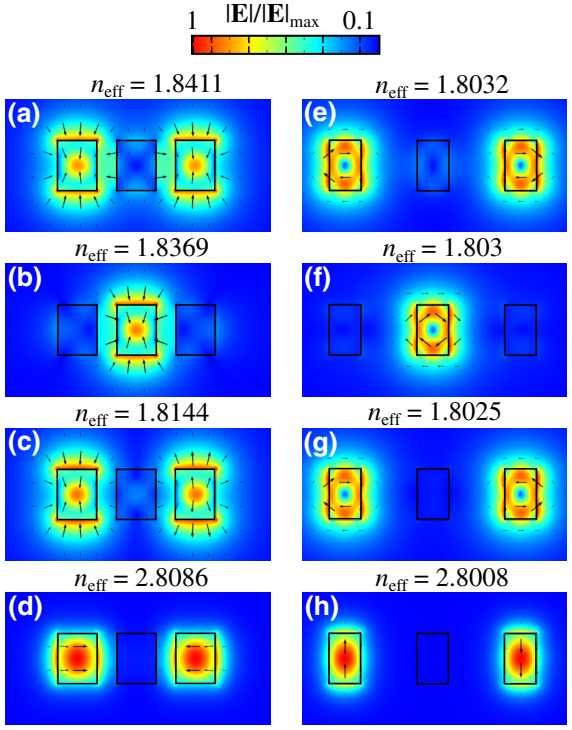

FIG. 8. The electric field amplitude profiles of the eigenmodes of the three-waveguide system, contributing to the RA- and AZ-mode excitations (left and right column, respectively) of the central waveguide. The arrows show the direction of the electric field. The waveguides in the left column have dimensions $w = 250$ nm, $h = 315$ nm, and $s = 120$ nm, while for the waveguides in the right column we have $w = 200$ nm, $h = 320$ nm, and $s = 350$ nm. The fields in (d),(h) are seen to be TE and TM polarized rather than RA or AZ polarized.

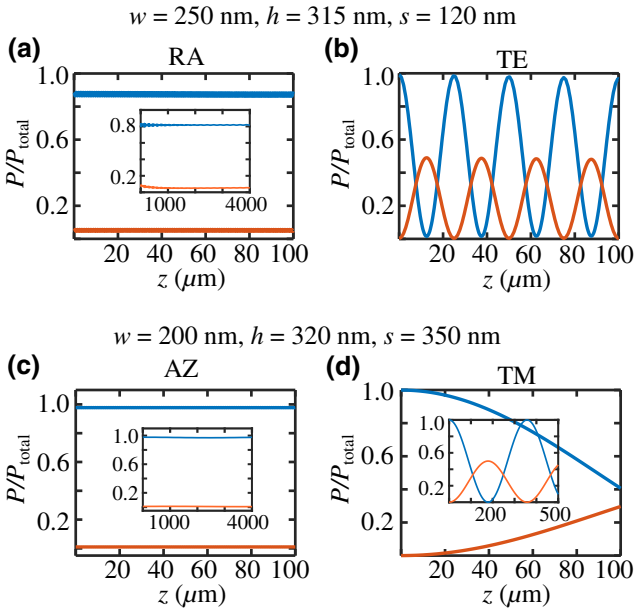

FIG. 9. Normalized power in the central (blue) and one of the side (red) waveguides as a function of propagation distance z in a three-waveguide system. The insets show the power transfer over a long propagation distance.

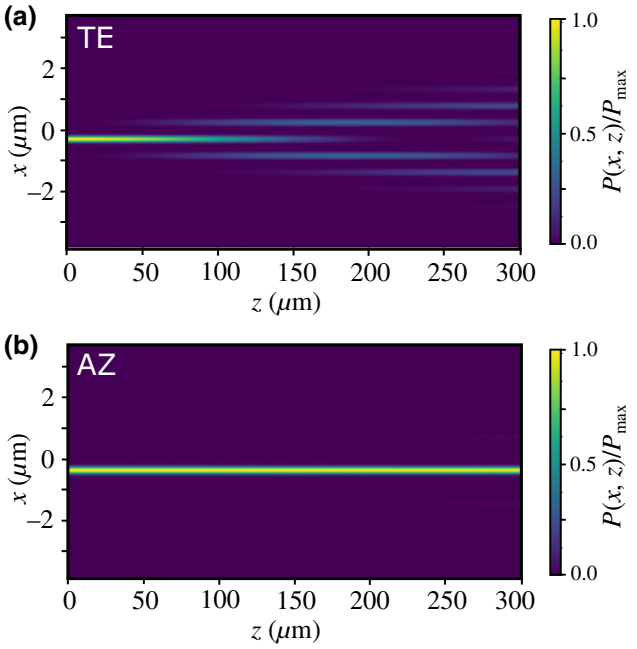

FIG. 10. Propagation of light coupled to a single waveguide of an array of ten closely spaced waveguides. The waveguide parameters are $w = 350$ nm, $h = 450$ nm, and $s = 200$ nm. At $\lambda = 1000$ nm, silicon is slightly absorbing, but in the present calculations, the absorption is neglected to better illustrate the crosstalk and its reduction.

seen in Fig. 10, if a TE mode is excited in the waveguide, the power spreads fast, escaping from the original waveguide after propagating for about 100 μm [Fig. 10(a)]. On the other hand, if an AZ mode is launched in the central waveguide, no coupling of light to other waveguides is observed for a propagation distance of 300 μm. This shows a remarkable advantage of the behavior of crosstalk-free higher-order modes over the fundamental modes.

To demonstrate this effect experimentally, an optical beam should be coupled to one of the waveguides, i.e., focused onto the entrance facet of a waveguide and having a radius of at most 300 nm (approximately 2 times smaller than the wavelength in glass). This focusing can be achieved by using a flat diffractive lens or a metalens [25,26]. The conversion of the TE mode to the AZ mode can be done right at the entrance of the waveguide. At the output of the system, the spread of light among the waveguides can be studied using a microscope or employing a similar flat-lens-based output coupler. In fact, the latter can be used to separate the signals arriving from the nanowaveguides and couple them to a larger waveguide array. The microlens will create a magnified image of the nanowaveguide output fields, which in the image plane will be coupled to the larger waveguide array. For example, if the waveguide system of Fig. 10 is in question, a magnification of 10 will make the necessary period of the large waveguide array equal to 5.5 μm.

III. CONCLUSIONS

In this work, we study the possibility to reduce the crosstalk between closely spaced waveguides by using higher-order modes, characterized by either radial or azimuthal polarizations. We find that, for a pair of waveguides, the crosstalk can be completely eliminated, even if the surface-to-surface distance between these waveguides is less than $\lambda/10$. This is enabled by equal effective mode indices of the symmetric and antisymmetric supermodes. The higher-order modes can be obtained from the fundamental modes with the help of a compact intrawaveguide phase shifter, similar to those of Ref. [20]. Directional couplers between crosstalk-free waveguides can be created by locally decreasing the waveguide separation or by another local disturbance. The couplers can be made exceptionally compact, since the waveguide separation is originally very small.

We also consider waveguide arrays with three and more waveguides and identify a range of parameter values for which the crosstalk is significantly reduced by using the aforementioned higher-order modes. To characterize large waveguide arrays, we propose an effective figure of merit that quantifies the efficiency of the crosstalk suppression. Our findings suggest that higher-order modes existing in waveguides of simple geometries, such as those with rectangular cross sections, could be used as a strategy for increasing the density of independent optical channels on a photonic chip and significantly reduce the footprint of photonic integrated circuits. The approach can be generalized to other types of optical waveguides, such as surface-mounted waveguides, photonic-crystal waveguides, and plasmonic-photonic waveguides. This, together with the development of waveguide couplers, resonators, and other on-chip components based on higher-order modes, defines the directions for the future research on the topic. Potential applications of crosstalk reduction by higher-order modes can be found in high-density integrated optical devices including, e.g., optical multiplexers, interconnects, and phased arrays [27–29].

ACKNOWLEDGMENTS

This work is funded by the Academy of Finland (308394). A significant part of the numerical calculations was performed using computational resources within the Aalto University School of Science "Science-IT" project. We also acknowledge the Academy of Finland Flagship Programme, Photonics Research and Innovation (Grant No. 320167, PREIN).

[1] W. N. Ye and Y. Xiong, Review of silicon photonics: History and recent advances, J. Mod. Opt. **60**, 1299 (2013).

[2] Z. Fang and C. Z. Zhao, Recent progress in silicon photonics: A review, Int. Sch. Res. Notices **2012**, 428690 (2012).

[3] D. Thomson, A. Zilkie, J. E. Bowers, T. Komljenovic, G. T. Reed, L. Vivien, D. Marris-Morini, E. Cassan, L. Virot, J.-M. Fédéli, J.-M. Hartmann, J. H. Schmid, D.-X. Xu, F. Boeuf, P. O'Brien, G. Z. Mashanovich, and M. Nedeljkovic, Roadmap on silicon photonics, J. Opt. **18**, 073003 (2016).

[4] A. H. Atabaki, S. Moazeni, F. Pavanello, H. Gevorgyan, J. Notaros, L. Alloatti, M. T. Wade, C. Sun, S. A. Kruger, H. Meng, K. A. Qubaisi, I. Wang, B. Zhang, A. Khilo, C. V. Baiocco, M. A. Popović, V. M. Stojanović, and R. J. Ram, Integrating photonics with silicon nanoelectronics for the next generation of systems on a chip, Nature **556**, 349 (2018).

[5] B. Szelag, K. Hassan, L. Adelmini, E. Ghegin, P. Rodriguez, F. Nemouchi, P. Brianceau, E. Vermande, A. Schembri, D. Carrara, P. Cavalie, F. Franchin, M.-C. Roure, L. Sanchez, C. Jany, and S. Olivier, Hybrid III–V silicon technology for laser integration on a 200-mm fully CMOS-compatible silicon photonics platform, IEEE J. Sel. Top. Quantum Electron. **25**, 1 (2019).

[6] N. Izhaky, M. T. Morse, S. Koehl, O. Cohen, D. Rubin, A. Barkai, G. Sarid, R. Cohen, and M. J. Paniccia, Development of CMOS-compatible integrated silicon photonics devices, IEEE J. Sel. Top. Quantum Electron. **12**, 1688 (2006).

[7] G. Veronis and S. Fan, Guided subwavelength plasmonic mode supported by a slot in a thin metal film, Opt. Lett. **30**, 3359 (2005).

[8] M. Z. Alam, J. S. Aitchison, and M. Mojahedi, A marriage of convenience: Hybridization of surface plasmon and dielectric waveguide modes, Laser Photonics Rev. **8**, 394 (2014).

[9] Y. Bian, Q. Ren, L. Kang, T. Yue, P. L. Werner, and D. H. Werner, Deep-subwavelength light transmission in hybrid nanowire-loaded silicon nano-rib waveguides, Photonics Res. **6**, 37 (2018).

[10] B. Zhang, Y. Bian, L. Ren, F. Guo, S.-Y. Tang, Z. Mao, X. Liu, J. Sun, J. Gong, X. Guo, and T. J. Huang, Hybrid dielectric-loaded nanoridge plasmonic waveguide for low-loss light transmission at the subwavelength scale, Sci. Rep. **7**, 1 (2017).

[11] W. Song, R. Gatdula, S. Abbaslou, M. Lu, A. Stein, W. Y. Lai, J. Provine, R. F. W. Pease, D. N. Christodoulides, and W. Jiang, High-density waveguide superlattices with low crosstalk, Nat. Commun. **6**, 1 (2015).

[12] R. Gatdula, S. Abbaslou, M. Lu, A. Stein, and W. Jiang, Guiding light in bent waveguide superlattices with low crosstalk, Optica **6**, 585 (2019).

[13] B. Shen, R. Polson, and R. Menon, Increasing the density of passive photonic-integrated circuits via nanophotonic cloaking, Nat. Commun. **7**, 1 (2016).

[14] Y. Yang, Y. Guo, Y. Huang, M. Pu, Y. Wang, X. Ma, X. Li, and X. Luo, Crosstalk reduction of integrated optical waveguides with nonuniform subwavelength silicon strips, Sci. Rep. **10**, 1 (2020).

[15] L. Wang, Z. Chen, H. Wang, A. Liu, P. Wang, T. Lin, X. Liu, and H. Lv, Design of a low-crosstalk half-wavelength pitch nano-structured silicon waveguide array, Opt. Lett. **44**, 3266 (2019).

[16] M. B. Mia, S. Z. Ahmed, I. Ahmed, Y. J. Lee, M. Qi, and S. Kim, Exceptional coupling in photonic anisotropic metamaterials for extremely low waveguide crosstalk, Optica **7**, 881 (2020).

[17] S. Jahani, S. Kim, J. Atkinson, J. C. Wirth, F. Kalhor, A. A. Noman, W. D. Newman, P. Shekhar, K. Han, V. Van, R. G. DeCorby, L. Chrostowski, M. Qi, and Z. Jacob, Controlling evanescent waves using silicon photonic all-dielectric metamaterials for dense integration, Nat. Commun. **9**, 1 (2018).

[18] M. A. Green, Self-consistent optical parameters of intrinsic silicon at 300 K including temperature coefficients, Sol. Energy Mater. Sol. Cells **92**, 1305 (2008).

[19] C. Li, D. Liu, and D. Dai, Multimode silicon photonics, Nanophotonics **8**, 227 (2019).

[20] B. E. Abu-Elmaaty, M. S. Sayed, R. K. Pokharel, and H. M. Shalaby, General silicon-on-insulator higher-order mode converter based on substrip dielectric waveguides, Appl. Opt. **58**, 1763 (2019).

[21] D. Chack, S. Hassan, and M. Qasim, Broadband and low crosstalk silicon on-chip mode converter and demultiplexer for mode division multiplexing, Appl. Opt. **59**, 3652 (2020).

[22] B. Saleh and M. Teich, *Fundamentals of Photonics*, Wiley Series in Pure and Applied Optics (Wiley, 2007).

[23] W.-P. Huang, Coupled-mode theory for optical waveguides: An overview, J. Opt. Soc. Am. A **11**, 963 (1994).

[24] H. Haus, W. Huang, S. Kawakami, and N. Whitaker, Coupled-mode theory of optical waveguides, J. Light. Technol. **5**, 16 (1987).

[25] Z. Wang, T. Li, A. Soman, D. Mao, T. Kananen, and T. Gu, On-chip wavefront shaping with dielectric metasurface, Nat. Commun. **10**, 1 (2019).

[26] R. Yang, Y. Shi, C. Dai, C. Wan, S. Wan, and Z. Li, On-chip metalenses based on one-dimensional gradient trench in the broadband visible, Opt. Lett. **45**, 5640 (2020).

[27] D. Dai and J. E. Bowers, Silicon-based on-chip multiplexing technologies and devices for peta-bit optical interconnects, Nanophotonics **3**, 283 (2014).

[28] S. Chung, H. Abediasl, and H. Hashemi, A monolithically integrated large-scale optical phased array in silicon-on-insulator CMOS, IEEE J. Solid-State Circuits **53**, 275 (2017).

[29] X. Yi, H. Zeng, S. Gao, and C. Qiu, Design of an ultra-compact low-crosstalk sinusoidal silicon waveguide array for optical phased array, Opt. Express **28**, 37505 (2020).